Monopolar Fault Reconfiguration of Bipolar Half Bridge Converter for Reliable Load Supply in DC Distribution System

Jianjun Ma, *Member, IEEE*, Miao Zhu, *Senior Member, IEEE*, Yunwei Li, *Fellow, IEEE*, and Xu Cai, *Senior Member, IEEE*

***Abstract*—This article proposed the concept of monopolar fault reconfiguration for bipolar dc distribution system realized with Bipolar Half Bridge (BiHB) converter. Monopolar fault reconfiguration oriented from bipolar high voltage direct current (HVdc) transmission grid. For dc distribution, the operation aim is to provide uninterrupted power supply to critical load under monopolar fault. It requires interfacing circuit with fault-tolerant capability as well as control design considering both bipolar and monopolar working mode. The proposed BiHB converter achieves mode switching by reconfiguring the converter switching pattern. Considering both monopolar and bipolar working mode, a bipolar modulation method is proposed for coordinate circuit design. Key influence factors relating to the transient voltage spikes have been identified, including the fault detection delay and the modulation method. Besides, to suppress the voltage spikes caused by monopolar fault, feed-forward compensation is adopted for smooth mode transition. The proposed BiHB converter and control strategy have been comparatively evaluated under fault protection and restoration. Uninterrupted power supply of load has been attained, in validation of the proposed monopolar fault reconfiguration concept.**

***Index Terms*—Bipolar dc system, bipolar operation, fault reconfiguration, feed-forward compensation, monopolar operation.**

I. Introduction

DC DISTRIBUTION system has been deemed as the enabling technology for integration of distributed energy source and reliable power supply [1], [2]. Among the various types of system structure, the bipolar dc system received special attention [3]–[9]. An illustration of the typical bipolar dc distribution system is shown in Fig. 1(a). It can halve the line-to-ground voltage level compared with monopolar dc counterpart, while maintaining the same line-to-line voltage level and transmission capacity. Besides, for distribution system, bipolar dc offers two voltage levels and more flexible load/source connections [3], [4].

However, due to the changeable working status of distribution system, line disconnection and short-circuit fault often appear, and pose challenges to reliable load supply [10], [11]. In this article, to ensure the continuous and reliable power supply of the critical load, a novel concept termed *monopolar fault reconfiguration* has been proposed with the consideration of the bipolar interfacing dc–dc converter. As shown in Fig. 1(a), when fault occurs on the positive pole, continuous power can still be supplied from the negative pole to guarantee uninterrupted

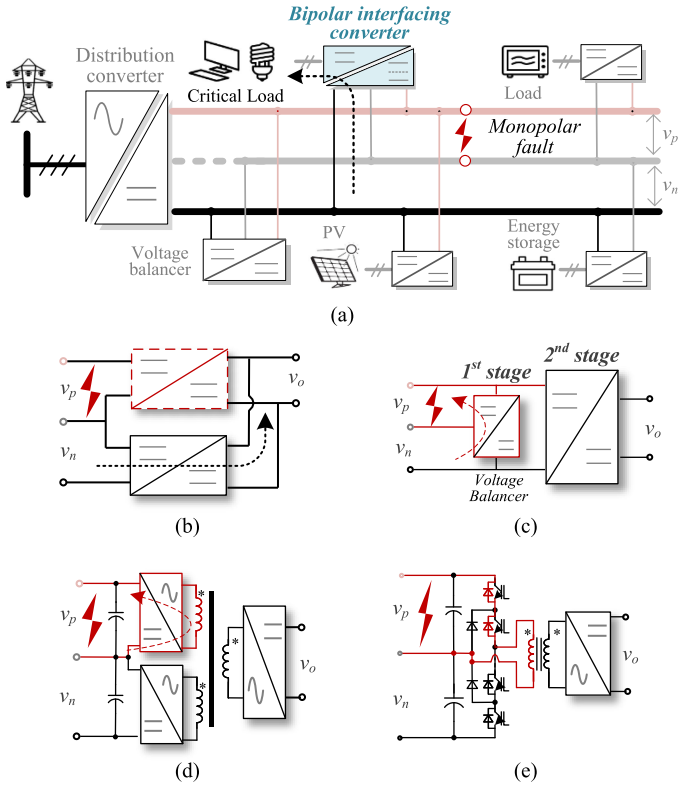

Fig. 1. Monopolar operation of bipolar dc distribution system. (a) System configuration. (b) Two-module bipolar circuit. (c) Integrated-balancing bipolar circuit. (d) Magnetic-coupled bipolar circuit. (e) NPC bipolar circuit.

Manuscript received November 7, 2021; revised February 12, 2022; accepted March 28, 2022. Date of publication April 13, 2022; date of current version May 23, 2022. This work was supported by Science and Technology Project of State Grid Corporation under Grant 52094021000M. Recommended for publication by Associate Editor M. H. Todorovic. *(Corresponding author: Miao Zhu.)*

Jianjun Ma, Miao Zhu, and Xu Cai are with the School of Electronic Information and Electrical Engineering, Shanghai Jiao Tong University, Shanghai 200240, China (e-mail: j.j.ma@sjtu.edu.cn; miaozhu@sjtu.edu.cn; xucai@sjtu.edu.cn).

Yunwei Li is with the Department of Electrical and Computer Engineering, University of Alberta, Edmonton, AB T6G 1H9, Canada (e-mail: yunwei.li@ualberta.ca).

Color versions of one or more figures in this article are available at https://doi.org/10.1109/TPEL.2022.3167100.

Digital Object Identifier 10.1109/TPEL.2022.3167100

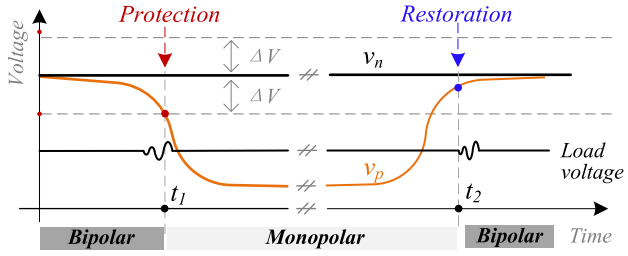

Fig. 2. Concept of monopolar fault reconfiguration for reliable load supply in bipolar dc system.

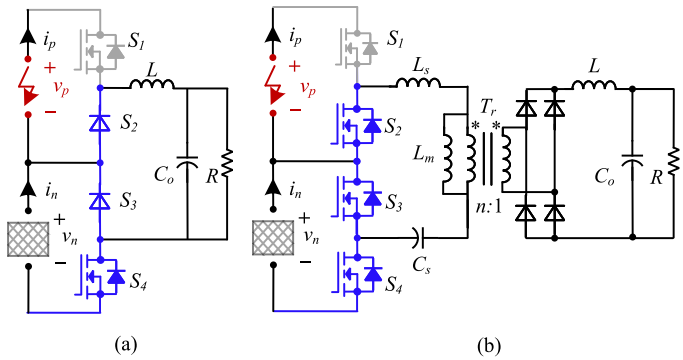

Fig. 3. Bipolar half bridge converter with monopolar fault reconfiguration capability. (a) Nonisolated converter. (b) Isolated converter.

power supply. When fault cleared, the converter is restored to bipolar mode for robust operation. As a result, uninterrupted power can be supplied to critical load and the distribution system is endowed with higher reliability. To ensure the abovementioned function, two key challenges are involved of, which are fault-tolerant bipolar circuit and multimode control.

Existing research on the bipolar dc–dc interfacing circuit can be grouped into four representative types, as shown in Fig. 1(b)–(e). The two modules circuit utilizing two separate converters and has a clear circuit structure, such as SEPIC-Cuk [12], Dual-DAB [13], etc. At the same time, this topology requires extra components with higher size and cost. Besides, power sharing between the two modules is also a key challenge, which further complicates the control. In Fig. 1(c), the integrated balancing circuit consists of two stages, with the first stage for power balancing and the second stage for voltage regulation. The buck–boost circuit is often adopted as the first stage unit and can be further merged with the second stage for more compact topology design [14]–[18]. In Fig. 1(d), the bipolar input ports are magnetically coupled with the load through a three-winding transformer [19]. When short-circuit fault occurs on one pole, the transformer is also shorted and leading to interrupted load supply. The bipolar converter can also be implemented with the diode neutral point clamped (NPC) circuit [20], as shown in Fig. 1(e). The NPC circuit can directly match the bipolar dc connections. Unfortunately, a common shortcoming of Fig. 1(c)–(e) is they are intolerable to monopolar fault. As shown in Fig. 1(c)–(e), when short circuit fault occurs on the positive pole, the converter feeds power to the fault point, and results in interrupted power supply. To guarantee reliable load supply, the bipolar converter should be tolerant to the monopolar short-circuit fault.

Apart from the converter design, the disturbance of mode transition should also be considered during monopolar fault reconfiguration. When considering the time sequence of fault protection and restoration, an illustration of the converter working mode is shown in Fig. 2. The voltage outage can be caused by short-circuit fault or line disconnection. When detecting the positive pole voltage v_p deviate from the normal range, the protection triggers and the converter works in monopolar mode. When the monopolar fault cleared, after receiving the restoration command, the converter recovers to bipolar mode. During that process, the control should maintain stable voltage regulation under the variation of working mode and input voltage.

The bipolar mode and monopolar mode are expected to have different dynamics. Traditional dual-loop control with rigid parameters often leads to instability in multimode operation [21]. A robust control scheme is necessary to maintain stable voltage regulation during the protection and restoration process. It is expected to simplify the control design in monopolar and bipolar modes with coordinate modulation design. Besides, during monopolar fault, the input voltage disturbance will be transferred to the output port. Feedforward control has been adopted for solving the input voltage disturbance [22], [23]. For monopolar fault protection in bipolar dc system, design, and performance of the corresponding feed-forward control remains to be explored.

To achieve monopolar fault reconfiguration of critical load, Bipolar Half Bridge (BiHB) converter and the corresponding modulation is proposed for coordinate circuit and control design. The rest of this article is organized as follows. In Section II, the operation of BiHB converter in monopolar mode and bipolar mode is analyzed and a novel bipolar modulation method is proposed. In Section III, circuit parameters are designed considering both bipolar and monopolar mode, and compared with conventional two-module circuit. In Section IV, control of BiHB converter is designed considering the dynamic difference in monopolar /bipolar modes and feedforward control is proposed to compensate the disturbance of short-circuit fault. The proposed circuit, modulation, and control design are comparatively evaluated with numerical simulations in Section IV and experimentally tested in Section V, in verification of monopolar fault reconfiguration function.

II. Operation of BiHB Converter

To ensure monopolar fault reconfiguration, the bipolar interfacing converter operates as a double-inputs single-output circuit with fault-tolerant operation capability. The corresponding circuit topology is first investigated.

A. Fault Tolerant BiHB Topology

The nonisolated and isolated BiHB converter circuits are shown in Fig. 3(a) and (b), respectively, where v_p and v_n are the input voltage at positive and negative pole, respectively.

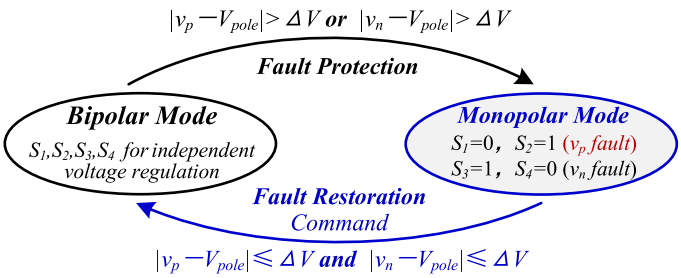

Fig. 4. State machine for monopolar fault reconfiguration of BiHB converter.

Different from the four switches three-level circuits [24]–[26], v_p, v_n are determined by the interfacing bipolar system.

During normal operation, v_p, v_n are the same as V_{pole}. When detecting the positive (negative) pole voltage v_p (v_n) deviate from the nominal value V_{pole} with the preset value (ΔV), the protection triggers by blocking the switch driving signals (S_1 for positive pole fault, S_4 for negative pole fault).

The protection logic of nonisolated and isolated BiHB converter are similar, and the state machine of BiHB converter is represented by Fig. 4.

The preset ΔV value relates with the sensitivity of fault detection and protection time-delay. If ΔV is selected too small, it will easily lead to false trigger of the protection. If ΔV is selected at large value, the bipolar converter should be robust to ride through the abnormal period, and therefore, has more stringent requirement on the control design. Other fault detection logic can also be adopted to reduce the fault detection time delay.

After the monopolar fault cleared, when receiving the restoration command, the driving signals of S_1–S_4 are reset to bipolar operation mode. Power is supplied from both the positive and negative pole, and the converter is readily prepared for consecutive fault.

Due to the similar requirement of monopolar reconfiguration, only the isolated BiHB converter is analyzed in this article. The following analysis can be easily applied for the nonisolated BiHB converter.

B. Monopolar Fault Operation Mode

To achieve coordinate design of the two working modes, the monopolar mode is first analyzed, due to relatively rigid modulation.

Without loss of generality, here assuming the short circuit fault occurs on the positive pole. After detecting the monopolar fault, S_1 is blocked and S_2 is constantly conducted. The BiHB converter is configured to monopolar mode and operating as asymmetrical half-bridge converter. The equivalent circuit and operating waveforms are shown in Fig. 5(a) and (b), respectively. In Fig. 5(a), v_{s2} and v_{s3} are the voltages across power switches S_2 and S_3, respectively. i_L is the inductor current. L is the inductance of the output filter. The primary winding resistance of the transformer is absorbed as a part of the equivalent series resistance (esr) r_c of the clamp capacitor with capacitance C_s, and the secondary winding resistance is merged into the esr r_L of the output inductor r_L. The leakage inductance L_s of transformer is expected at low value at the manufacture stage,

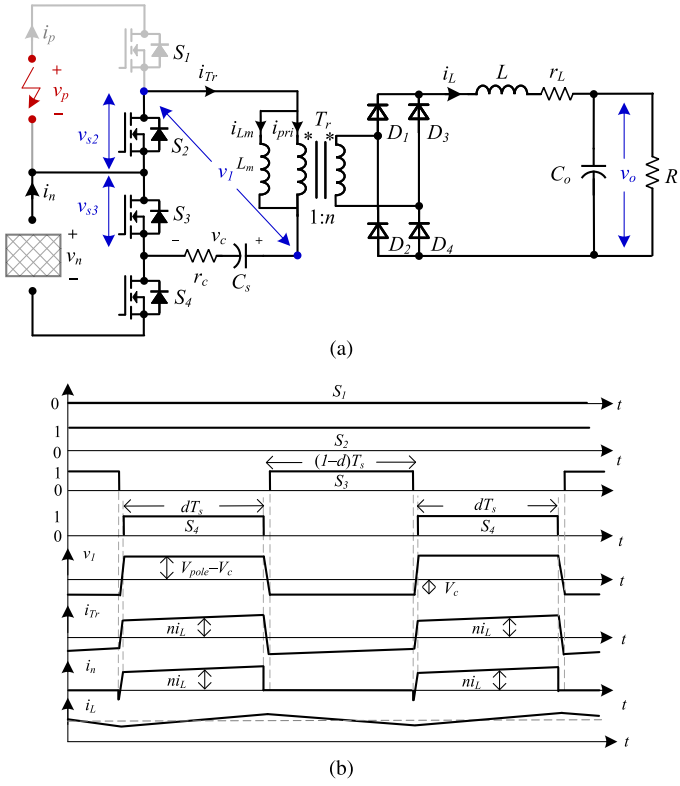

Fig. 5. BiHB converter operation in monopolar mode. (a) Schematic circuit. (b) Converter waveforms.

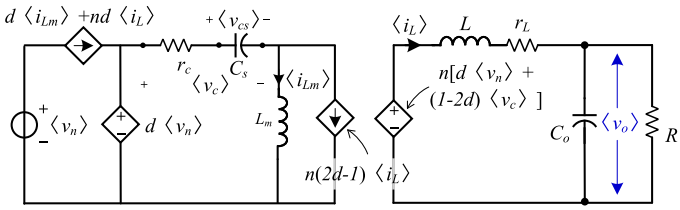

Fig. 6. Equivalent average model of BiHB converter in monopolar operation.

due to the resulting duty ratio loss. An evaluation on the influence of leakage inductance is analyzed in Section III.

As shown in Fig. 5(b), the duty ratio of S_4 and S_3 are in complementary and given as d and 1–d, respectively. Based on the voltage and current waveforms in Fig. 5, the average model of BiHB converter is shown in Fig. 6. The circuit variables are specified in Fig. 5(a), and$\langle\cdot\rangle$ indicates the average value of the circuit variables in one switching cycle.

The steady-state performance can be developed from the average model. When neglecting the influence of parasitic resistance (r_c, r_L), the average voltage v_{cs} of C_s, the output voltage v_o, and the average magnetizing current of i_{Lm} can be determined by voltage-second balance of L_m, L, and charge balance at C_s, respectively. According to Fig. 6, the relationship of average state variables v_{cs}, v_o, and i_{Lm} is given as

$$\begin{cases} \langle v_{cs}\rangle = d\,\langle v_n\rangle \\ \langle v_o\rangle = n\,[d\,\langle v_n\rangle + (1-2d)\,\langle v_c\rangle] \\ \langle i_{Lm}\rangle = n\,(1-2d)\,\langle i_L\rangle \end{cases}. \tag{1}$$

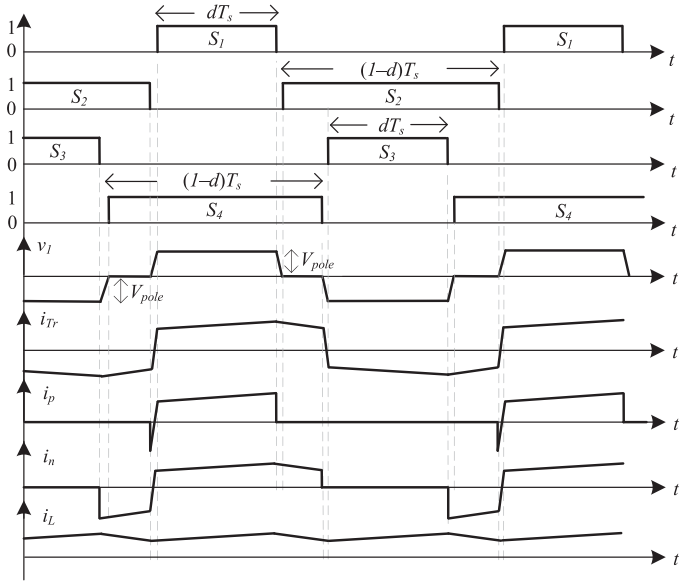

Fig. 7. Conventional three-level modulation waveforms of BiHB converter in bipolar mode.

Based on (1), the steady-state capacitor voltage V_{cs}, output voltage V_o, and magnetizing current I_{Lm} can be developed as (2), where D is the steady-state duty ratio

$$\begin{aligned} V_c &= DV_{\text{pole}},\ V_o = 2n\left[D\left(1-D\right)\right]V_{\text{pole}}, \\ I_{Lm} &= n\left(1-2D\right)I_L. \end{aligned} \tag{2}$$

The small-signal model in monopolar mode can also be obtained from Fig. 6, by linearizing the dependent sources under the small-signal assumption and given as (3), where "~" signifies the small-signal component of the respective circuit variables in Fig. 5(a)

$$\begin{cases} L_m \frac{d\tilde{i}_{Lm}}{dt} = \tilde{d}V_n + D\tilde{v}_n - \tilde{v}_c \\ C_s \frac{d\tilde{v}_{cs}}{dt} = \tilde{i}_{Lm} + n\left(2D-1\right)\tilde{i}_L + 2nI_L\tilde{d} \\ \tilde{v}_c = \tilde{v}_{cs} + r_c\left[\tilde{i}_{Lm} + n\left(2D-1\right)\tilde{i}_L + 2nI_L\tilde{d}\right] \\ L\frac{d\tilde{i}_L}{dt} = n\left[D\tilde{v}_n + \tilde{d}V_n - 2V_c\tilde{d} + (1-2D)\,\tilde{v}_c\right] - r_L\tilde{i}_L - \tilde{v}_o \\ C_o\frac{d\tilde{v}_o}{dt} = \tilde{i}_L - \frac{\tilde{v}_o}{R}. \end{cases} \tag{3}$$

C. Bipolar Normal Operation Mode

During bipolar operation, the positive and negative pole voltages v_p, v_n (see Fig. 3) are operating at the same value of V_{pole}. The driving signals of S_1 and S_3 can be assigned the same duty ratios and shifted by half switching cycle $T_s/2$, as shown in Fig. 7. This modulation method was previously applied for three-level converter [24]–[28], and can also be applied for the bipolar circuit. One main advantage of this modulation is zero dc bias of transformer. However, considering monopolar operation, the magnetizing current will be considered in transformer design and the advantage no longer holds.

One main drawback of this modulation is the unbalanced current flow through the positive pole and negative pole, as shown in i_p and i_n, respectively (see Fig. 7). The negative pole current i_n has longer charging and discharging process, and the different pole current will result in unbalanced positive and negative pole output power. Many works have been proposed on the current balancing control and it often requires more complex control design.

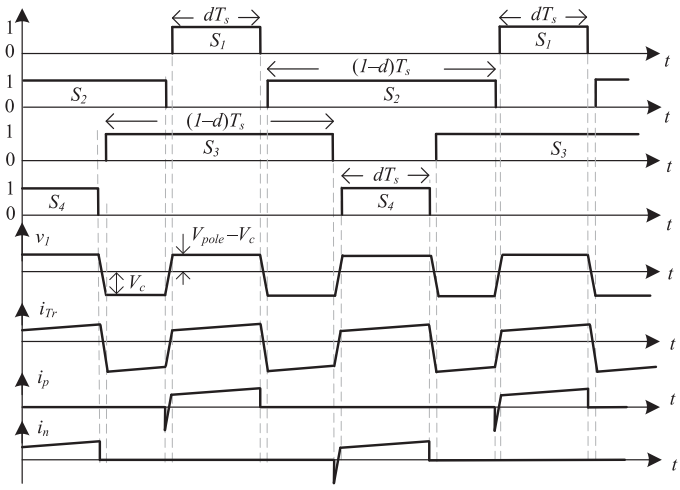

Fig. 8. Proposed bipolar modulation of BiHB converter in bipolar mode.

Moreover, with the conventional three-level modulation method, the dynamics of BiHB in bipolar mode also differs from the monopolar mode. With volt-second balance at the transformer *Tr*, the steady-state capacitor voltage V_c is given by

$$\begin{aligned} V_c &= DV_p + (1-D)\,V_n \\ &= V_{\text{pole}}. \end{aligned} \tag{4}$$

With volt-second balance at the inductor L, the steady-state output voltage V_o is given by

$$\begin{aligned} V_o &= n\left[D\left(2V_{\text{pole}} - V_c\right) + 2\left(1-D\right)\left(V_{\text{pole}} - V_c\right) + DV_c\right] \\ &= 2nDV_{\text{pole}}. \end{aligned} \tag{5}$$

The maximum output voltage is nV_{pole} and is two times larger than monopolar mode in (2). Thus, it will complicate the coordinate circuit design for two modes. Moreover, the capacitor voltage V_c in (4) is also higher than V_c in (1). It indicates higher voltage stress of C_s during bipolar operation.

As the alternative, when considering the monopolar operation, the proposed bipolar mode modulation is shown in Fig. 8. The duty ratios of $S_{1,}$ S_4 and $S_{2,}$ S_3 are in complementary and given as d and 1–d, respectively. The driving signals of S_1 and S_4 are shifted by half switching cycle.

The average model in bipolar mode is developed as Fig. 9. Like monopolar mode (see Fig. 6), the steady-state performance can be analyzed based on the average model. When neglecting the influence of parasitic resistance (r_c, r_L), the average voltage v_{cs} of C_s, the output voltage v_o, and the average magnetizing current of i_{Lm} can be determined by voltage-second balance of L_m, L, and charge balance at C_s, respectively. According to Fig. 9, the relationship of average state variables v_{cs}, v_o, and i_{Lm}

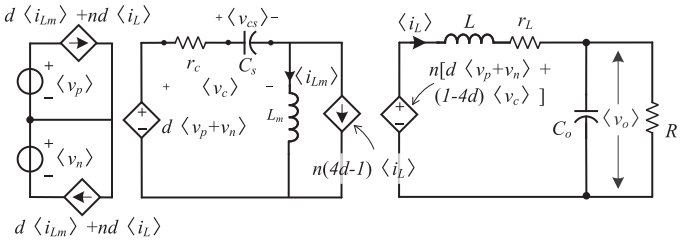

Fig. 9. Equivalent average model of BiHB converter in bipolar operation.

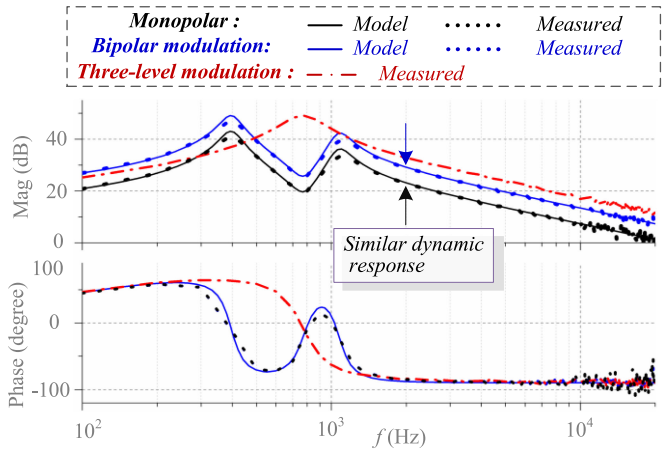

Fig. 10. i_L~d frequency response in monopolar and bipolar operation modes.

is given as

$$\begin{cases} \langle v_{cs}\rangle = d\left[\langle v_p\rangle + \langle v_n\rangle\right] \\ \langle v_o\rangle = n\left[d\langle v_p + v_n\rangle + (1-4d)\langle v_c\rangle\right] \\ \langle i_{Lm}\rangle = -n\left(4d-1\right)\langle i_L\rangle . \end{cases} \tag{6}$$

During bipolar operation, V_p and V_n are of the same value V_{pole}. Based on (1), the steady-state C_s capacitor voltage V_{cs}, output voltage V_o, and magnetizing current I_{Lm} can be developed as (7), where D is the steady-state duty ratio

$$\begin{aligned} &V_c = 2DV_{\text{pole}},\ V_o = V_o = 2n\left[2D\left(1-2D\right)\right]V_{\text{pole}}, \\ &I_{Lm} = n\left(1-4D\right)I_L. \end{aligned} \tag{7}$$

When comparing the waveforms of Fig. 8 with Fig. 5, the modulation in bipolar mode is similar with monopolar mode, except the equivalent switching frequency doubled in bipolar mode. As a result, when comparing (6), (7) with (1), (2), the steady-state output voltage V_o and inductor current i_L in bipolar mode can be developed by substituting D with $2D$ in monopolar mode. This similarity can also be observed between the two average models in Figs. 6 and 9.

Like monopolar mode, the small-signal model in bipolar mode can also be obtained from Fig. 9 by linearizing the dependent sources under the small-signal assumption and given as (8). The circuit variables are specified in Fig. 5.

In verification of the dynamic analysis, a comparison of i_L~d frequency responses between the small-signal model (4), (9) and the measured circuit response is shown in Fig. 10. For both monopolar and bipolar operation, the small-signal frequency response matches well with the measured results.

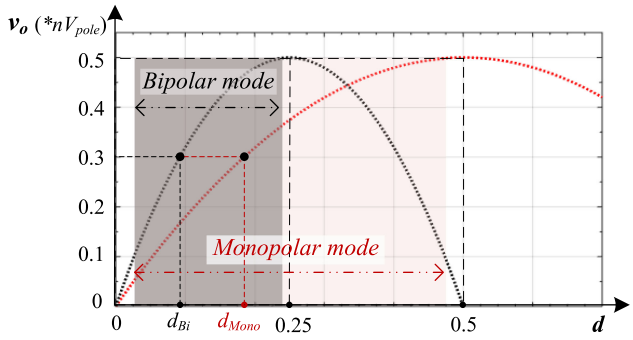

Fig. 11. BiHB converter regulation range in monopolar and bipolar modes.

It can also be observed that the i_L~d frequency response of monopolar and bipolar mode are similar. The only difference is the magnitude of $G_{iL\_d}(s)$ in bipolar mode is two times (6dB) higher than monopolar mode. An explanation is the duty ratio in monopolar mode is two times the equivalent duty ratio in bipolar mode. As a result, by substituting the duty ratio in bipolar mode with 1/2 duty ratio value in monopolar mode, the frequency response will be the same. This similarity will facilitate the following multimode control design:

$$\begin{cases} L_m\frac{d\tilde{i}_{Lm}}{dt} = \tilde{d}\left(V_p+V_n\right) + D\left(\tilde{v}_p+\tilde{v}_n\right) - \tilde{v}_c \\ C_s\frac{d\tilde{v}_{cs}}{dt} = \tilde{i}_{Lm} + n\left(4D-1\right)\tilde{i}_L + 4nI_L\tilde{d} \\ \tilde{v}_c = \tilde{v}_{cs} + r_c\left[\tilde{i}_{Lm} + n\left(4D-1\right)\tilde{i}_L + 4nI_L\tilde{d}\right] \\ L\frac{d\tilde{i}_L}{dt} = n\left[D\left(\tilde{v}_p+\tilde{v}_n\right)+\tilde{d}\left(V_p+V_n\right)-4V_c\tilde{d}+\left(1-4D\right)\tilde{v}_c\right] \\ \qquad -r_L\tilde{i}_L - \tilde{v}_o \\ C_o\frac{d\tilde{v}_o}{dt} = \tilde{i}_L - \frac{\tilde{v}_o}{R}. \end{cases} \tag{8}$$

In comparison, if adopting the conventional three-level modulation method (see Fig. 7), the i_L~d frequency response is also illustrated in Fig. 10. A large discrepancy exists between the bipolar mode and the monopolar mode. It has higher open-loop crossover frequency and the position of zeros and poles are also different. The dynamic difference will further complicate the control design and leads to potential instability. A more detailed analysis is given in Section IV and verified in Section V.

III. Parameter Selection and Comparison

To guarantee stable voltage regulation under both monopolar and bipolar mode, the circuit parameters should be designed with consideration of the two working modes collectively.

A. Parameter Selection

First, consider the transformer turns ratio. Based on (2) and (7), an illustration the output voltage (v_o) with the duty ratio (d) is shown in Fig. 11. The monopolar mode and the proposed bipolar mode have the same maximum output voltage $0.5nV_{\text{pole}}$. The output voltage reaches the maximum value at $d = 0.25$ and $d = 0.5$ for bipolar mode and monopolar mode, respectively. To ensure stable voltage regulation, in monopolar mode the duty ratio D_{Mono} should be constrained below 0.5. In bipolar mode, the duty ratio D_{Bi} should be constrained below 0.25.

TABLE I
CIRCUIT PARAMETERS OF BIHB CONVERTER

Parameter	Value
Input voltage (V_p,, V_n)	750 V (375 V, 375 V)
V_o	48 V
R	[5Ω, 20Ω]
Switching frequency f_s	50kHz
n	1: 2.5
L_m	5mH
L	300μH
C	50μF
C_s	20μF
r_c	0.1 Ω
r_L	0.15 Ω

Considering the voltage regulation range, the steady-state output voltage is designed at $0.3nV_{\text{pole}}$. Based on (2) and (7), the corresponding duty ratio in monopolar mode and bipolar mode can be determined as 0.09 and 0.18, respectively. For given input voltage V_{pole} and output voltage V_o, the transformer turns ratio n can, thus, be developed from (2). Besides, by combining (2) and (7), the average current of magnetizing inductance i_{Lm} is the same for monopolar and bipolar operation.

The inductors and capacitors are determined by the maximum ripple ratio. Assuming the steady-state duty ratio in monopolar mode and bipolar mode are D_{mono} and D_{bi}, respectively. The inductors and capacitors are developed by the given maximum current ripple ΔI_o, ΔI_{Lm} and voltage ripple ΔV_o, ΔV_{cs} in (9)–(12). According to (9)–(12), the circuit parameters are decided by the monopolar mode

$$L = \max\left[\frac{(0.5 - D_{\text{Mono}})\, V_o T_s}{\Delta I_o}, \frac{(0.25 - D_{Bi})\, V_o T_s}{\Delta I_o}\right] = \frac{(0.5 - D_{\text{Mono}})\, V_o T_s}{\Delta I_o} \tag{9}$$

$$L_m = \max\left[\frac{V_o T_s}{2n}\frac{1}{\Delta I_{Lm}}, \frac{V_o T_s}{4n}\frac{1}{\Delta I_{Lm}}\right] = \frac{V_o T_s}{2n}\frac{1}{\Delta I_{Lm}} \tag{10}$$

$$C_s = \max\left[\frac{V_o I_o T_s}{V_{\text{pole}}\Delta V_{cs}}, \frac{V_o I_o T_s}{2V_{\text{pole}}\Delta V_{cs}}\right] = \frac{V_o I_o T_s}{V_{\text{pole}}\Delta V_{cs}} \tag{11}$$

$$C_o = \max\left[\frac{\Delta I_o T_s}{8\Delta V_o}, \frac{\Delta I_o T_s}{16\Delta V_o}\right] = \frac{\Delta I_o T_s}{8\Delta V_o}. \tag{12}$$

When adopting larger parasitic inductor of transformer for zero-voltage switching, the abovementioned discussion and the average model in Figs. 6 and 9 can be modified considering the duty ratio loss. The converter efficiency can also be promoted when adopting other auxiliary circuit. Since the article mainly focuses on the fault protection and reconfiguration analysis, potential readers can refer to [27], [28], and [29]–[32] for more detailed power loss analysis on the three-level circuit and half-bridge circuit. The same work is not repeated in this article.

Based on (9)–(12), the designed circuit parameters are listed in Table I.

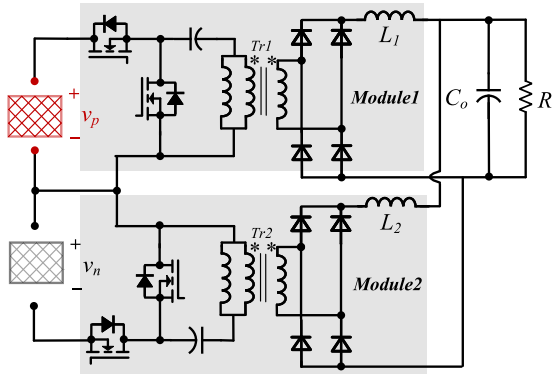

Fig. 12. Two-module bipolar circuit based on asymmetrical half-bridge converter.

TABLE II
COMPARISON OF BIHB CONVERTER WITH TWO-MODULE BIPOLAR CIRCUIT

Components	Items	BiHB (Fig. 3(b))	Two-modules (Fig. 12)
Diodes	Number	4	8
	Current rating	I_{load}	I_{load}
	Voltage rating	V_o	V_o
Power switches	Number	4	4
	Current rating	P_{load}/V_{pole}	P_{load}/V_{pole}
	Voltage rating	V_{pole}	V_{pole}
Capacitors	Number	2	3
	Voltage rating	V_{pole}, V_{load}	V_{pole}, V_{pole}, V_{load}
Inductors	Number	2	1
	Current rating	I_{load}	I_{load}
Transformers	Total Power rating	P_{load}	$2P_{load}$

B. Topology Comparison

Furthermore, to elaborate the characteristic of BiHB converter, the topology is compared with existing solutions. Few existing research covered the monopolar operation before. In Introduction, the topologies Fig. 1(c)–(e) are incapable of monopolar short circuit protection. As a result, the two-module circuit shown in Fig. 1(b) is adopted for comparison.

For a fair comparison, the power module is selected as asymmetrical half bridge converter, and the circuit is shown in Fig. 12. Without loss of generality, the secondary side is adopting the same diode bridge as Fig. 5(a). The asymmetrical half bridge converter can also be implemented with tapped transformer, and would not affect the comparison conclusion.

Assuming the total load power is P_{load}. To ensure uninterrupted power supply during monopolar fault, each of the power module rating is designed at P_{load}. A comparison of the converter components is listed in Table II. A distinctive advantage of the BiHB converter over the two-module circuit can be observed in component rating and number.

In addition, for the conventional two-module circuit, power sharing between the two modules is also a key challenge. In comparison, control of BiHB converter will be much easier

TABLE III
COMPARISON OF PROPOSED BIPOLAR MODULATION WITH CONVENTIONAL THREE-LEVEL MODULATION

Items	Three-level Modulation (conventional)	Bipolar Modulation (proposed)
DC current bias of transformer	Zero in bipolar mode Nonzero in monopolar mode	Nonzero in bipolar and monopolar mode
Voltage Stress of C_s	V_{pole}	Lower than V_{pole}
Current Stress of S_1~S_4	nI_L	nI_L+I_{Lm}
Voltage Stress of $S1$~$S4$	V_{pole}	V_{pole}
Voltage/current stress of diode	Nearly the same	
Spikes during monopolar protection	High and unavoidable	Nearly zero with low short fault detection delay
Control complexity	Potentially unstable	Relatively easy with dual-loop PI control
Efficiency	No absolute advantage for either of the modulation	

with the proposed modulation, which will be analyzed in the following section.

C. Modulation Comparison

Under the same BiHB converter circuit, the proposed bipolar modulation is also compared with conventional three-level modulation in terms of steady-state performance and dynamic response, as shown in Table III.

For steady-state performance, the three-level modulation has no dc current bias in bipolar operation and lower current stress of power switches. The bipolar modulation has lower voltage stress of capacitor C_s. Efficiency of two modulation schemes relate with the transformer and power switch parameter.

There is no absolute advantage for either of the modulations. When $d = 0.25$, the power loss will be the same. For transient performance, the proposed bipolar modulation can achieve smooth mode transition in open-loop. The close-loop control can also be easily implemented with dual-loop PI control, as analyzed in the following.

IV. CONTROL DESIGN

To ensure stable and smooth mode transition between monopolar and bipolar mode, the control design should consider dynamics of the two working modes collectively.

A. Multimode Feedback Control

First, consider the multimode feedback control design. Based on (3) and (8), the voltage loop $v_o \sim i_L$ transfer function are derived as $G_{vo\text{-}iL}(s)$ in (13). The two working modes have the same voltage-loop transfer function

$$G_{vo\_iL}(s) = \frac{1}{C_o s + R}. \tag{13}$$

TABLE IV
CONTROL PARAMETERS WITH DIFFERENT WORKING MODES

Working Mode	Bipolar Mode	Monopolar Mode
Current loop	k_{ip}=0.17, k_{ii}=6531	
Voltage loop	k_{vp}=0.16, k_{vi}=2088	

When neglecting the parasitic resistance r_c, r_L, the current-loop $i_L \sim d$ transfer function $G_{iL\text{-}d}(s)$ in monopolar and bipolar modes are given by (14) and (15) as shown bottom of the next page.

According to the analysis in Section II, the dynamic discrepancy between monopolar and bipolar mode is rigid 6dB magnitude difference at the $G_{iL\text{-}d}(s)$. To compensate the difference, the control output is multiplied with 1/2 at bipolar mode current-loop, as shown in Fig. 13. As a result, the voltage-loop and current-loop control parameters can be designed the same for monopolar and bipolar mode. For applications with low voltage quality requirement, the control diagram can operate in open-loop with given duty ratio d.

Here, the current-loop control is designed with crossover frequency $f_c = 10$ kHz (f_s/5). The close-loop $i_L \sim d$ frequency responses are shown in Fig. 14. It can be observed that in monopolar and bipolar mode, the close-loop $i_L \sim d$ frequency response overlaps with each other, in accordance with the abovementioned analysis. Similarly, the voltage-loop crossover frequency is placed at $f_v = 1$ kHz (f_c/10), and the designed control parameters are listed in Table IV.

In comparison, if adopting the conventional three-level modulation method (see Fig. 7), with the same current-loop PI control parameters (see Table III), the $i_L \sim d$ frequency response is also shown in Fig. 14. As can be observed, if adopting the conventional three-level modulation, the close-loop crossover frequency will reach 1/2 switching frequency (25 kHz). As a result, the control applicable for monopolar mode will lead to instability in bipolar mode, due to the dynamic difference. A further verification of the instability problem is given in Section V-B.

Considering the varying pole voltage before protection triggers and the varying load R, the designed control is checked for stable operation. As shown in Fig. 15, the close-loop eigenvalues all locate on left half plane, in verification of the designed gain/phase margin and converter stability. Besides, the eigenvalues in monopolar and bipolar modes overlaps with each other, in verification of the similar dynamics of the two working modes.

B. Influencing Factors on Smooth Mode Transition

Apart from stable voltage control, voltage spikes appear during fault protection. To investigate the influencing factors, here consider the open-loop mode transition. According to (3) and (8), in bipolar and monopolar mode, the converter model can be represented as A_{Bipolar} and $A_{\mathrm{Monopolar}}$, respectively, and x is

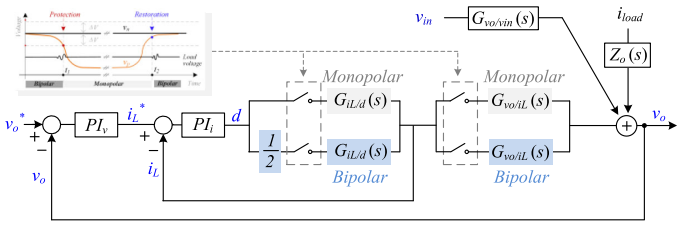

Fig. 13. Dual-loop control for two modes operation of BiHB converter.

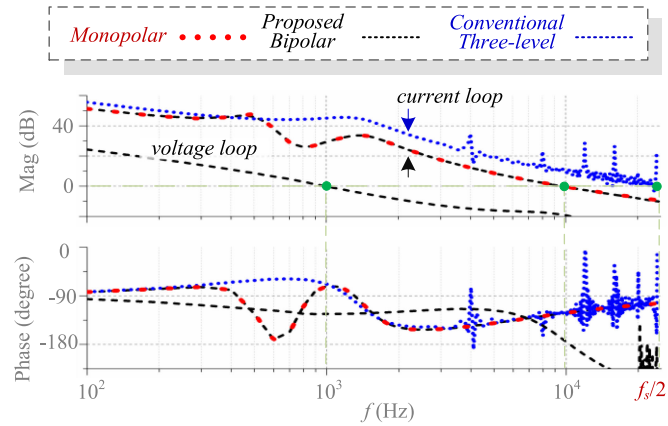

Fig. 14. Close-loop frequency response under different working modes.

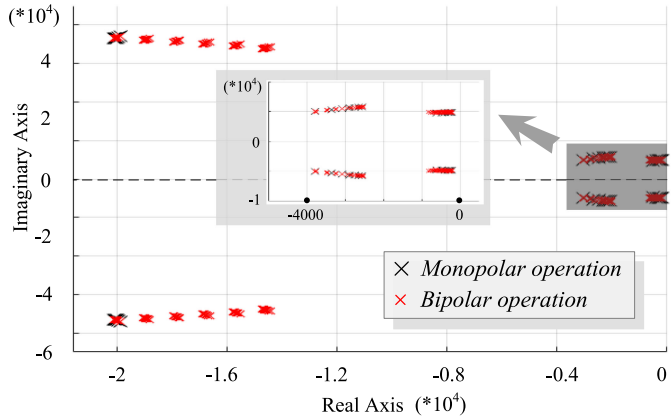

Fig. 15. Close-loop eigenvalues of BiHB converter with different working modes.

the state variable

$$\begin{cases} \dot{x} = A_{\text{Bipolar}} x\,, & \text{(Bipolar mode)} \\ \dot{x} = A_{\text{Monopolar}} x, & \text{(Monopolar mode)} \end{cases} \tag{16}$$

$$x = \begin{bmatrix} i_{Lm} & v_{cs} & v_c & i_L & v_o \end{bmatrix}. \tag{17}$$

Assuming the fault occurs at t = 0 and converter works in steady-state, with $A_{\text{Bipolar}}\, x(0) = 0$. At the instant of protection, (18) holds

$$\begin{aligned} \dot{x} &= A_{\text{Monopolar}} x\,(0) \\ &= \left[A_{\text{Monopolar}} - A_{Bi}\right] x\,(0)\,. \end{aligned} \tag{18}$$

With the proposed bipolar modulation (see Fig. 8), $A_{\text{Monopolar}} = A_{Bi}$, and $\dot{x} = 0$. It indicates no transient during mode transition. In comparison, if adopting the conventional three-level modulation (see Fig. 7), $A_{\text{Monopolar}} \neq A_{Bi}$. It indicates undesired spikes and transient during monopolar protection.

Even if adopting the proposed bipolar modulation, due to protection time delay, the input voltage varies. As a result, the model parameter changes with time and represented by $A_{\text{Monopolar}}(t)$ and $A_{\text{Bipolar}}(t)$. Assuming the fault occurs at $t = 0$ and the converter works in steady-state, with $A_{\text{Bipolar}}(0)x(0) = 0$. The protection triggers at $t = t_1$ and (19) holds

$$\begin{aligned} \dot{x} &= A_{\text{Monopolar}}\,(t_1)\,x\,(t_1) \\ &= A_{\text{Monopolar}}\,(t_1)\,x\,(t_1) - A_{\text{Bipolar}}\,(0)\,x\,(0) \\ &= \underbrace{\left[A_{\text{Monopolar}}\,(t_1) - A_{\text{Bipolar}}\,(0)\right]}_{\text{Input voltage variation}} x\,(t_1) \\ &\quad + \underbrace{\left[x\,(t_1) - x\,(0)\right]}_{\text{state change}} A_{\text{Bipolar}}\,(0)\,. \end{aligned} \tag{19}$$

Due to the variation of pole voltage before protection triggers $A_{\text{Monopolar}}(t_1) \neq A_{\text{Bipolar}}(0)$. The transient during mode transition will be introduced by input voltage variation and state change.

In summary, the undesired voltage spikes during mode transition can be suppressed by 1) adopting the proposed bipolar modulation method and 2) decreasing the fault detection time delay.

C. Smooth Mode Transition

Apart from stable voltage control, voltage overshoot appears during fault protection due to the input voltage variation and mode transition. Based on the converter model in (3) and (8), the influence of the input voltage v_p, v_n disturbance is described by Fig. 16, and represented by transfer function $G_{vo\_vin}(s)$. In Fig. 16, $G_{iL\_d}(s)$, $G_{vo\_iL}(s)$ denote the current-loop (i_L~d) and voltage-loop (v_o~i_L) transfer function, respectively. $G_{vo\_vin}(s)$ denote the disturbance of input voltage v_{in} with relation to the output voltage v_o.

To counteract the input voltage disturbance, an additional feedforward compensation branch of $H_{FF}(s)$ is introduced. As

Monopolar : $G_{iL\_d}(s)$

$$= \frac{\mathrm{n}(\mathrm{C_o R}s+1)\left[(2\mathrm{V_n}-2\mathrm{V_c}-2\mathrm{DV_n})+\left(2\mathrm{I_L L_m n}-4\mathrm{DI_L L_m n}\right)s+(\mathrm{C_s L_m V_n}-2\mathrm{C_s L_m V_c})s^2\right]}{\mathrm{R}+(\mathrm{L_o}+\mathrm{L_m n^2}-4\mathrm{DL_m n^2}+4\mathrm{D^2 L_m n^2})s+(\mathrm{C_o L_o R}+\mathrm{C_s L_m R}+\mathrm{C_o L_m R n^2}-4\mathrm{C_o DL_m R n^2}+4\mathrm{C_o D^2 L_m R n^2})s^2+\mathrm{C_s L_m L_o}s^3+\mathrm{C_o C_s L_m L_o R}s^4} \tag{14}$$

Bipolar : $G_{iL\_d}(s)$

$$= \frac{\mathrm{n}(\mathrm{C_o R}s+1)\left[(2\mathrm{V_p}+2\mathrm{V_n}-4\mathrm{V_c}-4\mathrm{DV_p}-4\mathrm{DV_n})+\left(4\mathrm{I_L L_m n}-16\mathrm{DI_L L_m n}\right)s+(\mathrm{C_s L_m V_p}+\mathrm{C_s L_m V_n}-4\mathrm{C_s L_m V_c})s^2\right]}{\mathrm{R}+(\mathrm{L_o}+\mathrm{L_m n^2}-8\mathrm{DL_m n^2}+16\mathrm{D^2 L_m n^2})s+(\mathrm{C_o L_o R}+\mathrm{C_s L_m R}+\mathrm{C_o L_m R n^2}-8\mathrm{C_o DL_m R n^2}+16\mathrm{C_o D^2 L_m R n^2})s^2+\mathrm{C_s L_m L_o}s^3+\mathrm{C_o C_s L_m L_o R}s^4}. \tag{15}$$

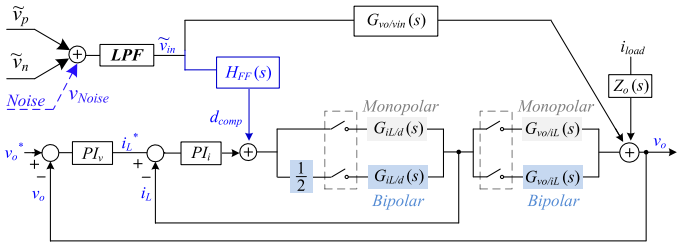

Fig. 16. Feed-forward compensation of BiHB converter considering input voltage disturbance.

shown in Fig. 16, relationship of v_{in} with v_o is given by

$$\tilde{v}_o = G_{vo\_vin}\tilde{v}_{in} + H_{FF}G_{vo\_iL}G_{iL\_d}\tilde{v}_{in}. \tag{20}$$

Therefore, to counteract the effect of input voltage disturbance, the feedforward compensation H_{FF} is given by

$$H_{FF} = -\frac{G_{vo\_vin}}{G_{vo\_iL}G_{iL\_d}}. \tag{21}$$

By substituting the transfer function of $G_{vo\_vin}(s)$, $G_{iL\_d}(s)$, and $G_{vo\_iL}(s)$ into the feedforward path H_{FF}, the compensation duty ratio d_{comp} can be derived. When neglecting the influence of parasitic resistance, d_{comp} is given as (22) shown at bottom of this page.

During monopolar dc fault, the input voltage disturbance often occurs at the low-frequency band, due the presence of line resistance and fault current limiting inductor. An approximation of (22) in the low-frequency band is given by (23). The steady-state duty ratio D in (23) can be derived based on (2) with the input voltage V_{pole} and reference output voltage. An approximation of D is by averaging the duty ratio output d values within last several switching cycles

$$\tilde{d}_{\text{comp}}(s)\Big|_{\text{Bi}} \approx \frac{2D - 4D^2}{(8D-2)(V_p + V_n)}\left[\tilde{v}_p(s) + \tilde{v}_n(s)\right]. \tag{23}$$

During practical implementation, the measured source voltage v_p, v_n can be further processed with low-pass filter. Besides, since the feedforward duty ratio d_{comp} relates with the source voltage variation, d_{comp} value should be reset after mode transition, due to the input source change.

In verification of the feedforward compensation performance, an illustration of the v_{in}~v_o frequency response is shown in Fig. 17. With the duty ratio compensation d_{comp} in (22), the magnitude of input voltage disturbance can be significantly reduced. Due to the neglect of parasitic resistance r_c, r_L, the disturbance is not fully compensated. In comparison, with the approximation in (23), similar frequency response can also be attained at the low frequency band below 300 Hz. The performance of the feedforward control is further tested in the following Sections.

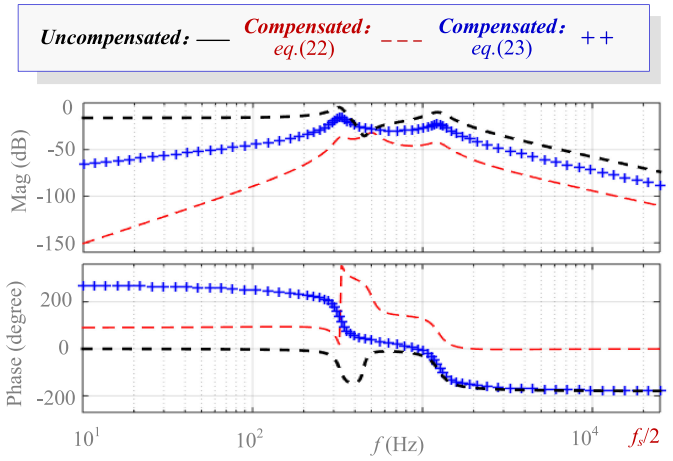

Fig. 17. v_{in}~ v_o frequency response with feedforward compensation.

V. Numerical Simulations

In verification of the monopolar fault reconfiguration concept, a case study with ±375 V/48 V BiHB converter is simulated. On the bipolar dc system side, the line resistance $r_{\text{line}} = 0.5\ \Omega$ and the line inductance $L_{\text{line}} = 20\ \mu$H. The detailed simulation parameters are listed in Table I, and the control parameters are in accordance with Table IV.

A. Fault Reconfiguration

Fig. 18 shows the dynamic simulation results of the BiHB converter. Initially, the positive and negative pole voltages v_p and v_n are near, and the BiHB converter operates in bipolar mode. The short circuit fault occurs on the positive pole with 10Ω equivalent grounding resistance, and the positive pole voltage v_p [see Fig. 18(g)] drops consequently.

In $t_1 = 0.03$ s, the positive pole voltage v_p drops below 0.7 V_{pole}. After detected the fault, S_1 is constantly blocked and S_2 is constantly ON, the switch voltage v_{s2} drops to 0 V [see Fig. 18(c)] and BiHB converter operates in monopolar mode. After the monopolar fault protection, the output voltage v_o remains constantly regulated, in verification of stable voltage regulation. Due to power balance, the negative pole current i_n doubled after entering monopolar mode.

The positive pole voltage v_p recovered at t = 0.05 s. After receiving the restoration command at $t = 0.06$ s, the driving signals of S_1 and S_2 are unlocked and the converter works in bipolar mode. During bipolar and monopolar modes, the PI control parameters remain the same. The output voltage v_o maintains constantly regulated during the fault recovery process. Moreover, during bipolar operation, the average output current i_p,i_n at the positive and negative pole are the same as 0.64 A, which indicates equal power sharing between the positive and negative pole.

$$\tilde{d}_{\text{comp}}(s)\Big|_{\text{Bi}} = \frac{\left(C_s L_m D s^2 + 2D - 4D^2\right)\left[\tilde{v}_p(s) + \tilde{v}_n(s)\right]}{\left(4V_c - V_p - V_n\right)C_s L_m s^2 + (16D-4)\,nI_L L_m s + (4D-2)(V_p + V_n) + 4V_c}. \tag{22}$$

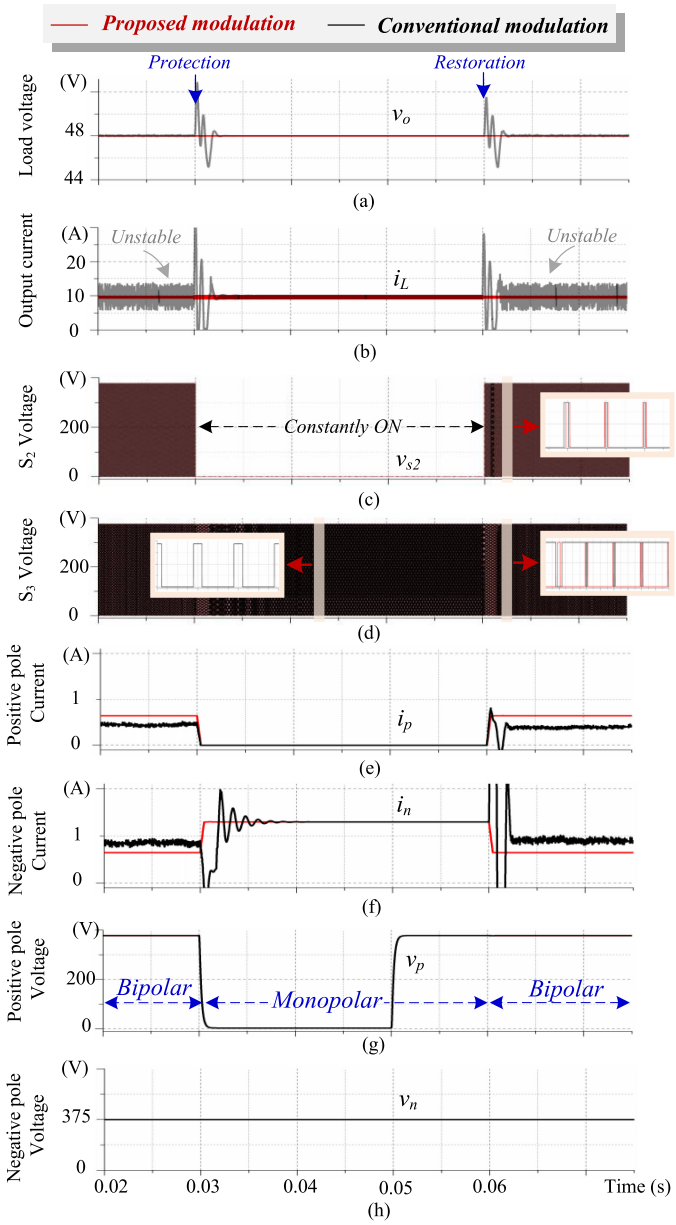

Fig. 18. Comparison of monopolar fault reconfiguration with different bipolar modulation methods.

The conventional three-level bipolar modulation method is also simulated for comparison. As shown in Fig. 18(a) and (b), the control design can maintain stable voltage regulation in monopolar mode. As soon as BiHB converter enters bipolar mode, the inductor current i_L and output voltage v_o becomes unstable. In accordance with the analysis in Section IV, the control stable for monopolar mode becomes unstable for conventional three-level bipolar modulation mode, due to the dynamic difference. Besides, the input current i_p, i_n at the positive pole and negative pole are also unequal. The conventional three-level modulation method will, thus, lead to unbalanced power sharing.

In summary, if adopting the proposed modulation method for bipolar mode, the control designed for monopolar mode is also applicable for bipolar mode. The output voltage v_o and inductor current i_L remains stable during monopolar fault protection and restoration. The proposed bipolar modulation method is more convenient for converter control design.

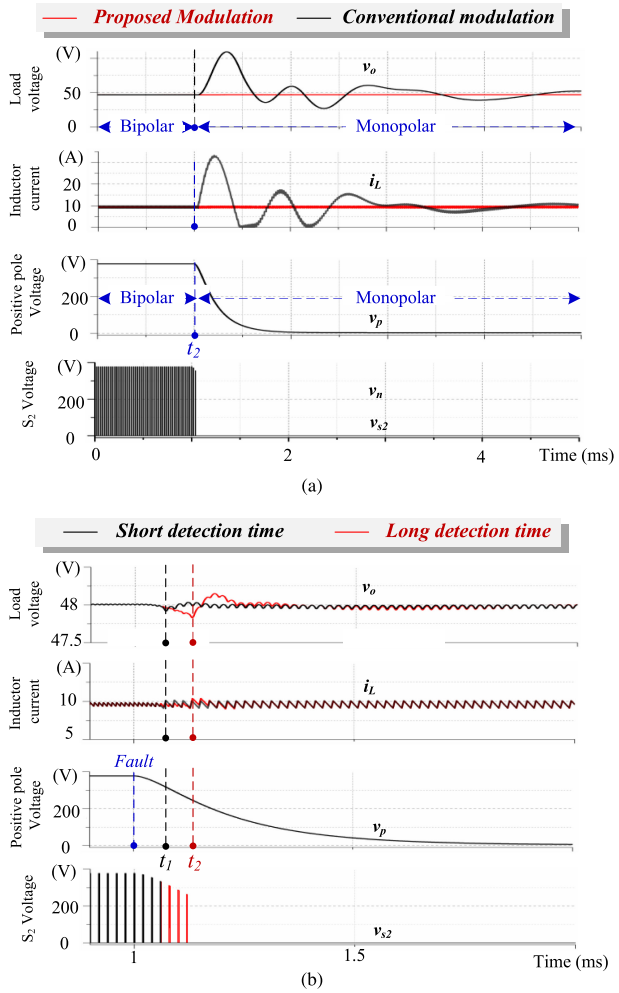

Fig. 19. Evaluation on influencing factors of mode transition voltage spikes. (a) Modulation method. (b) Fault detection delay.

B. Evaluation on Influence Factors

In verification of the influences of modulation method and fault detection time delay, a comparison of open-loop mode transition is shown in Fig. 19.

As shown in Fig. 19(a), monopolar protection triggers at the instant of monopolar fault. With the proposed bipolar modulation, near smooth mode transition can be observed. In comparison, with the conventional three-level modulation, large voltage spikes of output voltage v_o and high inductor current i_L overshoot can be observed.

A comparison of monopolar protection with different time delay is shown in Fig. 19(b). The longer time delay results in higher output voltage v_o spikes and higher inductor current i_L overshoot, in accordance with the analysis in Section IV.

C. Smooth Mode Transition

In verification of the feedforward compensation, the control design is tested under positive pole short circuit fault. As shown in Fig. 20, the short circuit fault occurs at $t_1 = 1$ ms and the

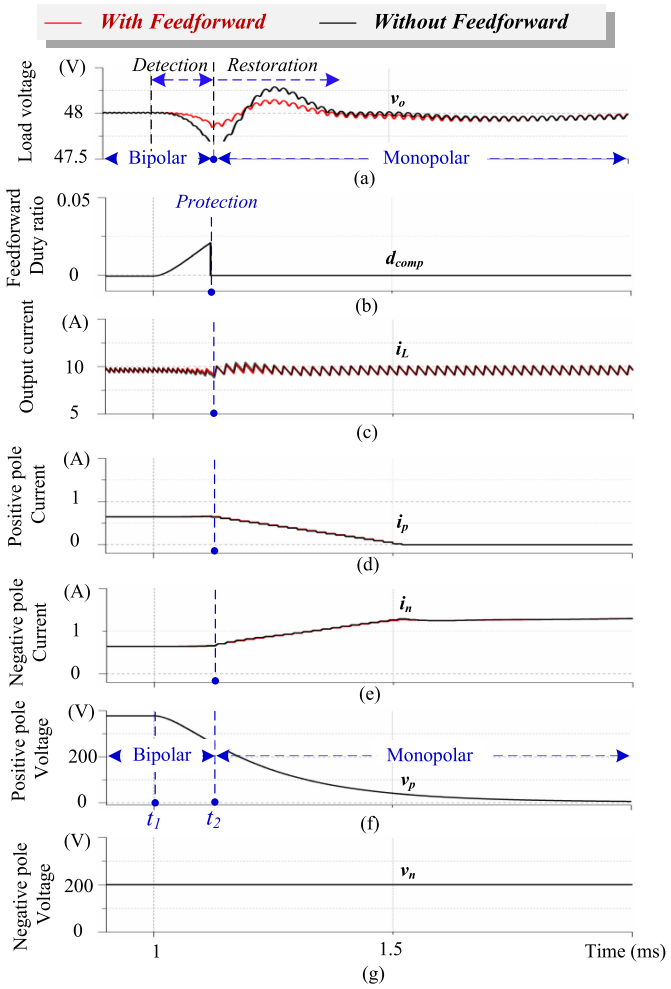

Fig. 20. Comparison of monopolar fault protection performance with/without feedforward compensation.

positive pole voltage v_p drops subsequently. At t_2, the protection triggers when detecting v_p drops below 240 V (0.7 times normal value), and the working mode changes from bipolar to monopolar. It will lead to drop of output voltage v_o and high voltage overshoot in monopolar mode.

To compensate the voltage disturbance caused by monopolar fault, the feedforward control proposed in Section IV is adopted. As shown in Fig. 20(b), during the detection period, the compensation duty ratio d_{comp} is generated with the feedforward compensation. Deviation of the output voltage v_o can be reduced before the monopolar protection triggers. The recovery time in monopolar mode can also be reduced, in support of the design aim. After t_2, when entering monopolar mode, the compensation duty ratio d_{comp} drops to 0 due to no voltage disturbance at the negative pole.

VI. Experimental Verifications

In verification of BiHB converter and the monopolar fault reconfiguration concept, an experimental prototype has been built. The detailed circuit parameters are listed Table V.

TABLE V
Circuit Parameters of BiHB Converter

Parameter	Value
Input voltage (V_p, V_n)	96 V (48 V, 48V)
V_o	15 V
R	[5Ω, 20Ω]
Switching frequency f_s	50kHz
n	1:1
L_m	500μH
L	200μH
C	110μF
C_s	200μF
r_c	0.1 Ω
r_L	0.15 Ω

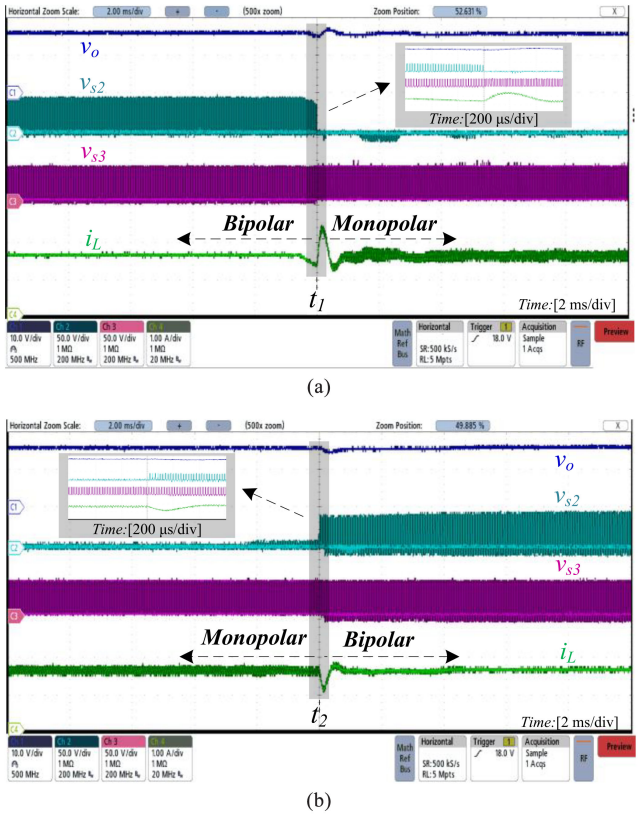

Fig. 21. Voltage regulation under monopolar short-circuit fault reconfiguration. (a) Fault protection. (b) Fault restoration.

A. Fault Protection and Restoration

The converter is first tested for monopolar short circuit protection. During normal operation, the input voltage at the positive pole and negative pole are the same of 48 V. The voltages across the power switch S_2 and S_3 are determined by the positive and negative pole voltages, and shown as v_{s2}, v_{s3}, respectively.

As shown in Fig. 21(a), when short circuit fault occurs on the positive pole at time t_1, the switch S_2 voltage v_{s2} drops as a consequence. The protection triggers when detecting the positive pole voltage drops below 0.7 times normal value (35 V), and the switch S_2 is constantly closed. The converter switches to monopolar mode. Compared with bipolar mode, the current

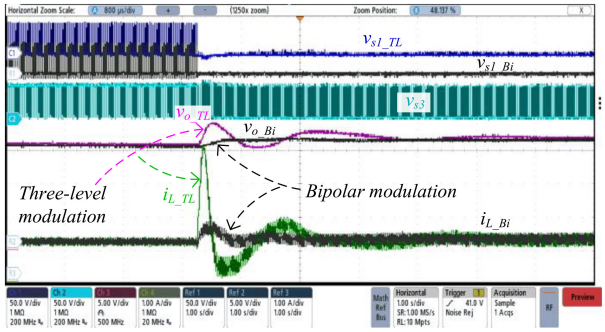

(a)

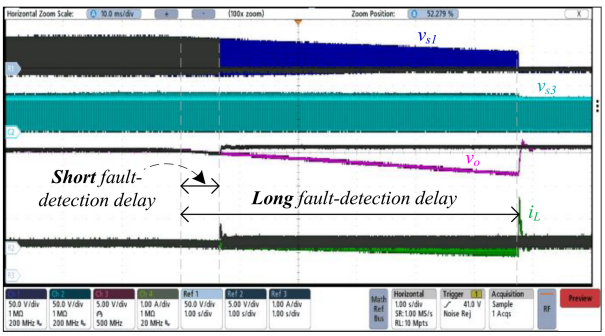

(b)

Fig. 22. Evaluation on influencing factors of mode transition spikes. (a) Modulation method. (b) Fault detection delay.

ripple in monopolar mode nearly doubled, in accordance with the analysis in Section III.

During the fault protection process, the output voltage v_o stays constantly regulated, in verification of the protection scheme and robust control design.

When the monopolar short circuit fault cleared, the input voltage v_p recovered to normal value. As shown in Fig. 21(b), after receiving the restoration command at time t_2, the driving signals of S_1 and S_2 are unlocked and the converter returns to bipolar mode.

During the mode transition, the PI control parameters stay the same values. With the proposed modulation method, the control maintains stable output voltage v_o regulation during the fault recovery process. After the restoration, the converter is tolerant to successive monopolar fault, in verification of the resilient load supply design aim.

B. Evaluation on Influencing Factors

In verification of the influences of different modulation method and fault detection time delay, the open-loop mode transition are comparatively evaluated in Fig. 22.

In Fig. 22(a), the protection triggers with the same fault detection delay. Compared with the proposed bipolar modulation, the three-level modulation has higher output voltage spike v_{o_TL} and current overshoot i_{L_TL}. The result supports the advantages of the proposed bipolar modulation during mode transition.

In Fig. 22(b), the modulation is selected the same of the proposed bipolar modulation. The longer time delay leading to larger output voltage deviation and higher current spikes, in verification of the analysis results in Section IV-B.

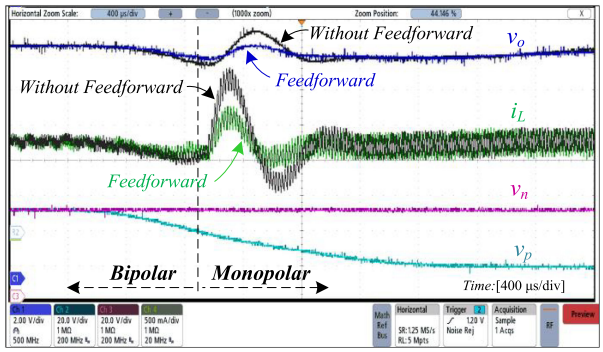

Fig. 23. Comparison of BiHB converter performance during mode transition with/without feedforward compensation.

C. Smooth Mode Transition

To suppress the disturbance caused by monopolar fault, the feedforward control is adopted. As shown in Fig. 23, in emulation of short circuit fault, the positive pole voltage v_p decreases from 48 V to 8 V in 2 ms. The protection triggers when detecting v_p drops below 35 V (0.7 V_{pole}), and the working mode changes from bipolar to monopolar mode.

During that process, the output voltage v_o first drops due to the positive pole voltage v_p deviation. After the monopolar protection, high overshoots of output voltage, and inductor current can be observed.

In comparison, with the proposed feedforward compensation, the output voltage v_o have lower voltage deviation before monopolar protection. The total recovery time and current overshoot can also be reduced, in validation of the design aim.

VII. Conclusion

In duality of monopolar operation in bipolar transmission grid, the concept of bipolar fault reconfiguration is first proposed for dc distribution system and validated with the BiHB converter. Main contributions of this article are as follows.

1) To guarantee reliable load power supply, uninterrupted power can be supplied from the nonfault pole to critical load. This function is proposed as bipolar fault reconfiguration.
2) For BiHB converter, the bipolar modulation method is first proposed to achieve coordinated circuit and control design in both monopolar and bipolar modes.
3) Key influence factors of bipolar reconfiguration transient have been identified, including modulation methods in monopolar/bipolar mode and fault detection time delay.
4) To suppress the disturbance during bipolar reconfiguration, feedforward compensation is proposed for smooth mode transition.

The abovementioned designs are validated through comparative numerical simulations and experimental results, in verification of the bipolar fault reconfiguration concept and the BiHB converter implementation.

This article also has limitations: Scope of the article mainly focuses on the verification of monopolar fault reconfiguration concept. Efficiency of the BiHB converter can be further promoted. Besides, the half-bridge circuit is suitable for low to medium power level. For higher power applications, potential multiphase topology with monopolar fault reconfiguration capability deserves further investigation.

REFERENCES

[1] CIGRE WG C6.31 "Medium voltage direct current (MVDC) grid feasibility study," CIGRE Tech. Brochure 793, Paris, France, Feb. 2020.

[2] D. Boroyevich, I. Cvetkovic, R. Burgos, and D. Dong, "Intergrid: A future electronic energy network," *IEEE J. Emerg. Sel. Topics Power Electron.*, vol. 1, no. 3, pp. 127–138, Sep. 2013.

[3] S. Rivera, R. Lizana F., S. Kouro, T. Dragičević, and B. Wu, "Bipolar DC power conversion: State-of-the-art and emerging technologies," *IEEE J. Emerg. Sel. Topics Power Electron.*, vol. 9, no. 2, pp. 1192–1204, Apr. 2021.

[4] H. Kakigano, Y. Miura, and T. Ise, "Low-voltage bipolar-type dc microgrid for super high quality distribution," *IEEE Trans. Power Electron.*, vol. 25, no. 12, pp. 3066–3075, Dec. 2010.

[5] T. Dragičević, X. Lu, J. C. Vasquez, and J. M. Guerrero, "DC microgrids—Part II: A review of power architectures, applications, and standardization issues," *IEEE Trans. Power Electron.*, vol. 31, no. 5, pp. 3528–3549, May 2016.

[6] J. Lago and M. L. Heldwein, "Operation and control-oriented modeling of a power converter for current balancing and stability improvement of dc active distribution networks," *IEEE Trans. Power Electron.*, vol. 26, no. 3, pp. 877–885, Mar. 2011.

[7] Y. Gu, W. Li, and X. He, "Analysis and control of bipolar LVDC grid with DC symmetrical component method," *IEEE Trans. Power Syst.*, vol. 31, no. 1, pp. 685–694, Jan. 2016..

[8] L. Tan, B. Wu, S. Rivera, and V. Yaramasu, "Comprehensive DC power balance management in high-power three-level DC-DC converter for electric vehicle fast charging," *IEEE Trans. Power Electron.*, vol. 31, no. 1, pp. 89–100, Jan. 2016.

[9] J. Ma, M. Zhu, Y. W. Li, and X. Cai, "DC substation for DC grid—Part II: Hierarchical control strategy and verifications," *IEEE Trans. Power Electron.*, vol. 34, no. 9, pp. 8682–8696, Sep. 2019.

[10] A. A. S. Emhemed and G. M. Burt, "An advanced protection scheme for enabling an LVDC last mile distribution network," *IEEE Trans. Smart Grid,* vol. 5, no. 5, pp. 2602–2609, Sep. 2014.

[11] J. Park and J. Candelaria, "Fault detection and isolation in low-voltage DC-Bus microgrid system," *IEEE Trans. Power Del.*, vol. 28, no. 2, pp. 779–787, Apr. 2013.

[12] M. B. Ferrera, S. P. Litr´an, E. D. Aranda, and J. M. A. M´arquez, "A converter for bipolar dc link based on SEPIC-Cuk combination," *IEEE Trans. Power Electron.*, vol. 30, no. 12, pp. 6483–6487, Dec. 2015.

[13] H. Zhu, M. Zhu, J. Zhang, X. Cai, and N. Dai, "Topology and operation mechanism of monopolarto-bipolar DC-DC converter interface for DC grid," in *Proc. IEEE 8th Int. Power Electron. Motion Control Conf.*, 2016, pp. 3728–3733.

[14] J.-Y. Lee, H.-S. Kim, and J.-H. Jung, "Enhanced dual-active-bridge dc-dc converter for balancing bipolar voltage level of dc distribution system," *IEEE Trans. Ind. Electron.*, vol. 67, no. 12, pp. 10399–10409, Dec. 2020.

[15] F. Wang, Z. Lei, X. Xu, and X. Shu, "Topology deduction and analysis of voltage balancers for DC microgrid," *IEEE J. Emerg. Sel. Topics Power Electron.*, vol. 5, no. 2, pp. 672–680, Jun. 2017.

[16] S. Kim, H. Cha, and H. -G. Kim, "High-efficiency voltage balancer having DC–DC converter function for EV charging station," *IEEE J. Emerg. Sel. Topics Power Electron.*, vol. 9, no. 1, pp. 812–821, Feb. 2021.

[17] X. Zhang, C. Gong, and Z. Yao, "Three-level dc converter for balancing DC 800-V voltage," *IEEE Trans. Power Electron.*, vol. 30, no. 7, pp. 3499–3507, Jul. 2015.

[18] B. Li *et al.*, "DC/DC converter for bipolar LVdc system with integrated voltage balance capability," *IEEE Trans. Power Electron.*, vol. 36, no. 5, pp. 5415–5424, May 2021.

[19] S. Ouyang, J. Liu, S. Song, X. Chen, Y. Yang, and H. Wu, "Solid state transformer for low-voltage distribution system with DC/DC stage-controlled split-capacitor," in *Proc. IEEE Energy Convers. Congr. Expo.*, 2019, pp. 5805–5809.

[20] J. Lee, Y. Cho, and J. Jung, "Single-stage voltage balancer with high frequency isolation for bipolar LVDC distribution system," *IEEE Trans.*

[21] J. Ma, M. Zhu, Y. Li, and X. Cai, "Dynamic analysis of multimode buck–boost converter: An LPV system model point of view," *IEEE Trans. Power Electron.*, vol. 36, no. 7, pp. 8539–8551, Jul. 2021.

[22] M. Chen and J. Sun, "Feedforward current control of boost single-phase PFC converters," *IEEE Trans. Power Electron.*, vol. 21, no. 2, pp. 338–345, Mar. 2006.

[23] B. Arbetter and D. Maksimovic, "Feedforward pulse width modulators for switching power converters," *IEEE Trans. Power Electron.*, vol. 12, no. 2, pp. 361–368, Mar. 1997.

[24] V. Yaramasu, B. Wu, S. Alepuz, and S. Kouro, "Predictive control for low-voltage ride-through enhancement of three-level-boost and NPC-Converter-Based PMSG wind turbine," *IEEE Trans. Ind. Electron.*, vol. 61, no. 12, pp. 6832–6843, Dec. 2014.

[25] I. Barbi, R. Gules, R. Redl, and N. O. Sokal, "DC/DC converter: Four switches Vpk = Vin /2, capacitive turn-off snubbing, ZV turn-on," *IEEE Trans. Power Electron.*, vol. 19, no. 4, pp. 918–927, Jul. 2004.

[26] C. Lu, W. Hu, and F. C. Lee, "Neutral-point voltage balancing methods of series-half-bridge LLC converter for solid state transformer," *IEEE Trans. Power Electron.*, vol. 36, no. 6, pp. 7060–7073, Jun. 2021.

[27] D. Liu, F. Deng, Q. Zhang, and Z. Chen, "Periodically swapping modulation (PSM) strategy for three-level (TL) DC/DC converters with balanced switch currents," *IEEE Trans. Ind. Electron.*, vol. 65, no. 1, pp. 412–423, Jan. 2018.

[28] X. Yu, K. Jin, and Z. Liu, "Capacitor voltage control strategy for half-bridge three-level DC/DC converter," *IEEE Trans. Power Electron.*, vol. 29, no. 4, pp. 1557–1561, Apr. 2014.

[29] J. Han, J. Kim, B. Lee, J. Lai, and G. Moon, "High-Efficiency asymmetrical half-bridge converter with a new coupled inductor rectifier (CIR)," *IEEE Trans. Power Electron.*, vol. 34, no. 12, pp. 11541–11552, Dec. 2019.

[30] G. Di Capua, S. A. Shirsavar, M. A. Hallworth, and N. Femia, "An enhanced model for small-signal analysis of the phase-shifted full-bridge converter," *IEEE Trans. Power Electron.,* vol. 30, no. 3, pp. 1567–1576, Mar. 2015.

[31] B. Choi, W. Lim, Sanghyun Bang, and Seungwon Choi, "Small-signal analysis and control design of asymmetrical half-bridge DC-DC converters," *IEEE Trans. Ind. Electron.*, vol. 53, no. 2, pp. 511–520, Apr. 2006.

[32] M. Arias, M. F. Diaz, D. G. Lamar, F. M. Fernández Linera, and J. Sebastián, "Small-signal and large-signal analysis of the two-transformer asymmetrical half-bridge converter operating in continuous conduction mode," *IEEE Trans. Power Electron.*, vol. 29, no. 7, pp. 3547–3562, Jul. 2014.

Jianjun Ma (Member, IEEE) received the B.S. degree from Xi'an Jiaotong University, Xi'an, China, in 2013 and the Ph.D. degree from Shanghai Jiao Tong University, Shanghai, China, in 2019, both in electrical engineering.

Since Jan. 2020, he has been a Postdoctoral Research Fellow with the Department of Electrical Engineering, Shanghai Jiao Tong University, Shanghai, China. His research interests include renewable energy integration, dc distributed power system, and dc grid.

Miao Zhu (Senior Member, IEEE) received the B.Sc. degree from Southeast University, Nanjing, China, in 2001 and the Ph.D. degree from Nanyang Technological University, Singapore, in 2009, both in electrical engineering.

During 2001–2002, he was an Assistant Engineer with Wuxi Power Supply Company, State Grid of China. From 2008 to 2009, he was with Meiden Asia Pte., Ltd., Singapore, as an R&D Engineer. After that, he had been a Scientist with the Experimental Power Grid Centre, A∗STAR, Singapore. In Aug. 2012, he was with the Shanghai Jiao Tong University (SJTU), China, as Research Professor with the honor title of Distinguished Researcher. He is currently the Professor with the Department of Electrical Engineering, SJTU and the Vice Director with the State Energy Smart Grid (Shanghai) R&D Centre. Since 2018, he has been the Vice Chairman of both IEEE PELS Shanghai Chapter and IEEE IES Shanghai Chapter. He is a regular reviewer for a number of academic journals, and has authored and coauthored nearly 90 papers in refereed journals and conferences proceedings. His research interests include power converters, renewable energy generation, dc distributed power system, and dc grid.

Prof. Zhu is the recipient of 2009 IEEE Power Electronics Society Prize Letter Award. In 2010, he was awarded the World Future Foundation Ph.D. Prize in Environmental and Sustainability Research. In 2018, he was appointed as the

Yunwei Li (Fellow, IEEE) received the B.Sc. degree in electrical engineering from Tianjin University, Tianjin, China, in 2002 and the Ph.D. degree in electrical engineering from Nanyang Technological University, Singapore, in 2006.

In 2005, he was a Visiting Scholar with Aalborg University, Denmark. From 2006 to 2007, he was a Postdoctoral Research Fellow with Ryerson University, Canada. In 2007, he was with Rockwell Automation Canada before he was with the University of Alberta, Canada in the same year. Since then, he has been with University of Alberta, where he is a Professor now. His research interests include distributed generation, microgrid, renewable energy, high powerconverters, and electric motor drives.

Dr. Li serves as Editor-in-Chief for IEEE Transactions on Power Electronics Letters. Prior to that, he was Associate Editor for the IEEE TRANSACTIONS ON POWER ELECTRONICS, IEEE TRANSACTIONS ON INDUSTRIAL ELECTRONICS, IEEE TRANSACTIONS ON SMART GRID, and IEEE JOURNAL OF EMERGING AND SELECTED TOPICS IN POWER ELECTRONICS. He was the recipient of the Richard M. Bass Outstanding Young Power Electronics Engineer Award from IEEE Power Electronics Society in 2013 and the second prize paper award of IEEE TRANSACTIONS ON POWER ELECTRONICS in 2014. He is listed as a Highly Cited Researcher by the Web of Science Group.

Xu Cai (Senior Member, IEEE) received the B.Eng. degree from Southeast University, Nanjing, China, in 1983, and the M.Eng. and Ph.D. degrees from China University of Mining and Technology, Jiangsu, China, in 1988 and 2000, respectively, all in electrical engineering.

He was with the Department of Electrical Engineering, China University of Mining and Technology, as an Associate Professor from 1989 to 2001. He was the Vice Director of the State Energy Smart Grid R&D Center, Shanghai, China, from 2010 to 2013. He has been with Shanghai Jiao Tong University, Shanghai, as a Professor since 2002, where he has also been the Director of the Wind Power Research Center since 2008. His current research interests include power electronics and renewable energy exploitation and utilization, including wind power converters, wind turbine control system, large power battery storage systems, clustering of wind farms and its control system, and grid integration.